Extremely Efficient White Organic Light-Emitting Diodes for General Lighting

Qing-Dong Ou, Lei Zhou, Yan-Qing Li, Su Shen, Jing-De Chen, Chi Li, Qian-Kun Wang, Shuit-Tong Lee, and Jian-Xin Tang**

Highly power-efficient white organic light-emitting diodes (OLEDs) are still challenging to make for applications in high-quality displays and general lighting due to optical confinement and energy loss during electron-photon conversion. Here, an efficient white OLED structure is shown that combines deterministic aperiodic nanostructures for broadband quasi-omnidirectional light extraction and a multilayer energy cascade structure for energy-efficient photon generation. The external quantum efficiency and power efficiency are raised to 54.6% and 123.4 lm W^{-1} at 1000 cd m^{-2}. An extremely small roll-off in efficiency at high luminance is also obtained, yielding a striking value of 106.5 lm W^{-1} at 5000 cd m^{-2}. In addition to a substantial increase in efficiency, this device structure simultaneously offers the superiority of angular color stability over the visible wavelength range compared to conventional OLEDs. It is anticipated that these findings could open up new opportunities to promote white OLEDs for commercial applications.

1. Introduction

White organic light emitting diodes (OLEDs) are gaining increasing importance in applications including full-color display panels, wearable intelligent electronics, and ecofriendly interior lighting due to their steadily improving efficiency and their other desirable features including superior white color balance, fascinating flexibility, and wide viewing angle.[1–8] The highest power efficiency (η_{PE}) of state-of-the-art white OLEDs reported in the scientific literature has exceeded 90 lm W^{-1} beyond fluorescent tube efficiency.[2] Nevertheless, further enhancements in η_{PE} of white OLEDs are urgently required,[8–13] as they are far from the theoretical efficiency limit of 249 lm W^{-1}.[14]

To achieve power-efficient white OLEDs, high internal quantum efficiency, low operating voltage, and high light out-coupling efficiency must be simultaneously addressed during the conversion of electrical energy to photons.[2–5,7–13] Internal quantum efficiency for the electron-photon conversion already approaches ≈100% in OLEDs with the use of phosphorescence or thermally activated delayed fluorescence, which allows the harvesting of both singlet and triplet excitons generated by electrical injection.[10–13] A number of strategies for low-operating-voltage technologies have also been adopted with the use of the buffer layer and electrical doping for multilayer energy level matching, or the control of the molecular orientation, which can remarkably reduce the energy loss during charge injection and transport processes.[8,9,15–18] Another challenge is the limited light out-coupling, which is as low as ≈20% in the conventional OLED architecture.[19] The majority of the internally generated light is confined in the substrate and waveguide modes due to the index mismatch of multiple layers or is lost by absorption and surface plasmon polaritons of the metal electrode.[20,21]

The development of light extraction technologies is thus an increasingly popular strategy to enhance the overall device efficiency in OLEDs. Various photonic structures have been proposed to the appropriate interfaces, including the use of microlens arrays,[22–24] high-refractive-index substrates,[2,25] sub-wavelength photonic crystals,[26,27] Bragg diffraction gratings,[28,29] low-index grids,[5] spontaneously formed buckles,[7] surface plasmons,[30–32] etc. However, many attempts with periodic structures are hindered from practical adoption due to limited response to specific emission wavelengths or viewing angles. Considering the desirable features of full-color displays and interior lighting, an alternative for enhancing light out-coupling is the use of quasicrystalline or random structures, which offer unique advantages for broadband, broad-angle light manipulation due to their richer Fourier spectra.[33] However, previous reports have not fully exploited their potential for device applications and OLEDs with substantial efficiency enhancement have not yet been shown.

Q.-D. Ou, L. Zhou, Prof. Y.-Q. Li, J.-D. Chen, C. Li, Q.-K. Wang, Prof. S.-T. Lee, Prof. J.-X. Tang
Institute of Functional Nano & Soft Materials (FUNSOM)
Jiangsu Key Laboratory for Carbon-Based Functional Materials & Devices
Collaborative Innovation Center of Suzhou Nano Science and Technology
Soochow University
Suzhou 215123, China
E-mail: yqli@suda.edu.cn; jxtang@suda.edu.cn
Prof. S. Shen
College of Physics
Optoelectronics and Energy
Soochow University
Suzhou, 215006, China

DOI: 10.1002/adfm.201402026

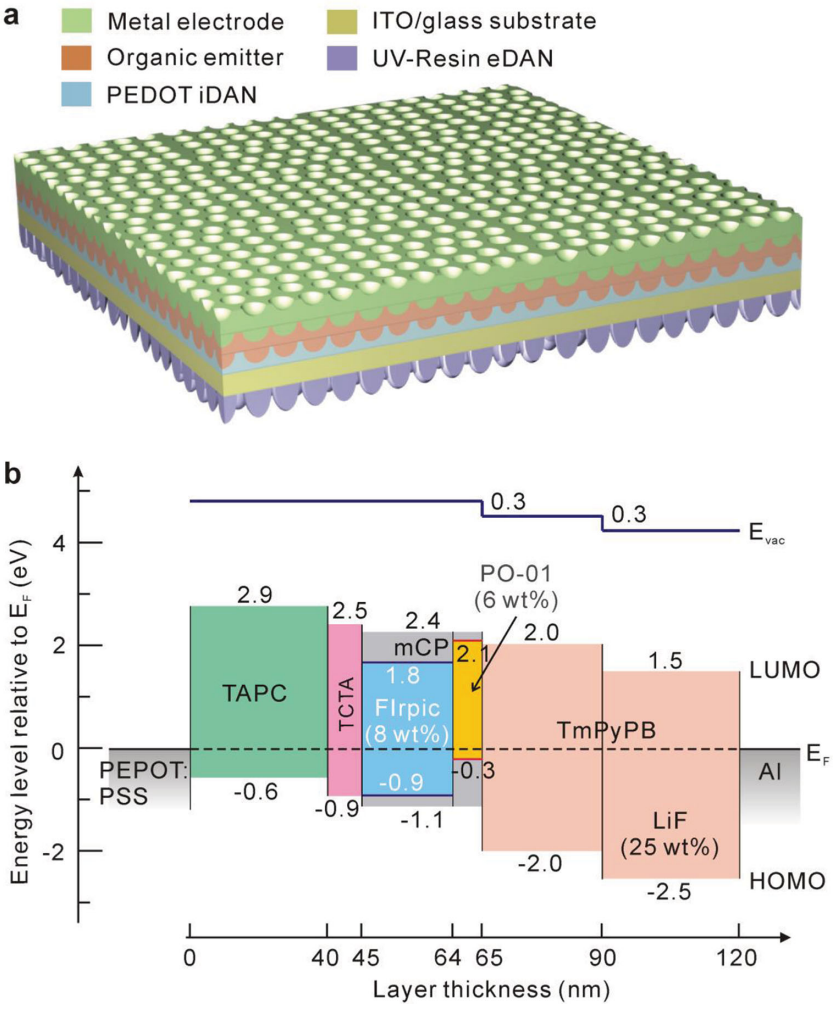

Figure 1. Device structure and energy level diagram of white OLEDs. a) Schematic of the white OLED, in which both sides of the ITO glass substrate is patterned with DANs. The organic layers and the metal electrode are then subsequently deposited onto the substrate. b) Energy level diagram of the organic emitter with the alignment of Fermi level across the interface, which is on basis of UPS measurements. Note that the formation of interface dipoles is present.

Here, we demonstrate an efficient white OLED structure using a novel approach for broadband quasi-omnidirectional light extraction with reduced energy loss during electron-photon conversion. The key feature is the use of deterministic aperiodic nanostructures (DANs) with long-range disorder and short-range order that significantly reduces the optical confinement without spectral distortion. By combining an optimized phosphorescent emitter with a multilayer energy cascade structure that minimizes the energetic and Ohmic losses for energy-efficient photon generation, a record efficiency for white OLEDs is achieved. The external quantum efficiency (η_{EQE}) and η_{PE} are improved to 54.6% and 123.4 lm W^{-1} at 1000 cd m^{-2}, respectively, which are two times those from conventional devices in a flat structure. Moreover, this OLED structure offers an extremely small roll-off in efficiency at high luminance and superior angular color stability over the visible wavelength range. We anticipate that this approach may stimulate the development of white OLEDs in the use of full-color displays and lighting sources.

2. Results and Discussion

2.1. Device Design

Figure 1a presents a schematic diagram of the device structure constructed with DANs by adopting a soft nanoimprint lithography (SNIL) technique (see the Experimental Section and Supporting Information Figure S1 for details). The internal DAN in the nanohoneycomb style is transferred to the poly(3,4-ethylene dioxythiophene):polystyrene sulfonic acid (PEDOT:PSS) layer on top of an indium tin oxide (ITO) surface before organic layer deposition (hereafter termed iDAN), while the external DAN in the nanocone style is patterned to UV-curable resin on glass surface (hereafter termed eDAN), which is conducted after encapsulating the device with a cap glass to prevent the damage to the formed nanostructures under pressure. The scalable fabrication methods using SNIL are fully amenable to large-area mass-manufacturing of OLED panels.

The white organic emitter is constructed with complementary blue and yellow phosphorescent emissions, consisting of 40 nm-thick di-[4-(N,N-ditolyl-amino)-phenyl]cyclohexane (TAPC) for hole transport, 5 nm-thick 4,44′,4′′-tris-(N-carbazolyl)-triphenylamine (TCTA) for hole injection, 19 nm-thick 8 wt% bis(3,5-difluoro-2-(2-pyridyl)phenyl-(2-carboxypyridyl)iridium(III) (FIrpic):N,N′-dicarbazolyl-3,5-benzene (mCP) for blue emission, 1 nm-thick 6 wt% Iridium(III) bis(4-phenylthieno [3,2-c]pyridinato-N,C2′) acetylacetonate (PO-01):mCP for yellow emission, 25 nm-thick 1,3,5-tri[(3-pyridyl)-phen-3-yl]benzene (TmPyPB) for electron transport and hole blocking, and then 30 nm-thick 25 wt% LiF:TmPyPB for electron injection (see Experimental Section and Supporting Information Figure S2 for chemical structures). Figure 1b depicts the energy level diagram of the highest occupied molecular orbital (HOMO), the lowest unoccupied molecular orbital (LUMO), and the vacuum level (E_{vac}) for all materials relative to the Fermi level (E_F), as determined using ultraviolet photoelectron spectroscopy (UPS) measurements for the HOMO and E_{vac} values (Supporting Information Figure S3) and using the optical gap for the LUMO values. The Fermi level alignment is used here for estimating the interface energetics because of the possible presence of the vacuum level discontinuity.[34]

2.2. Characteristics of DANs

Figure 2a,b show the atomic force microscopy (AFM) images of iDAN patterned on PEDOT:PSS and eDAN patterned on UV-curable resin, displaying both sub-wavelength structures and

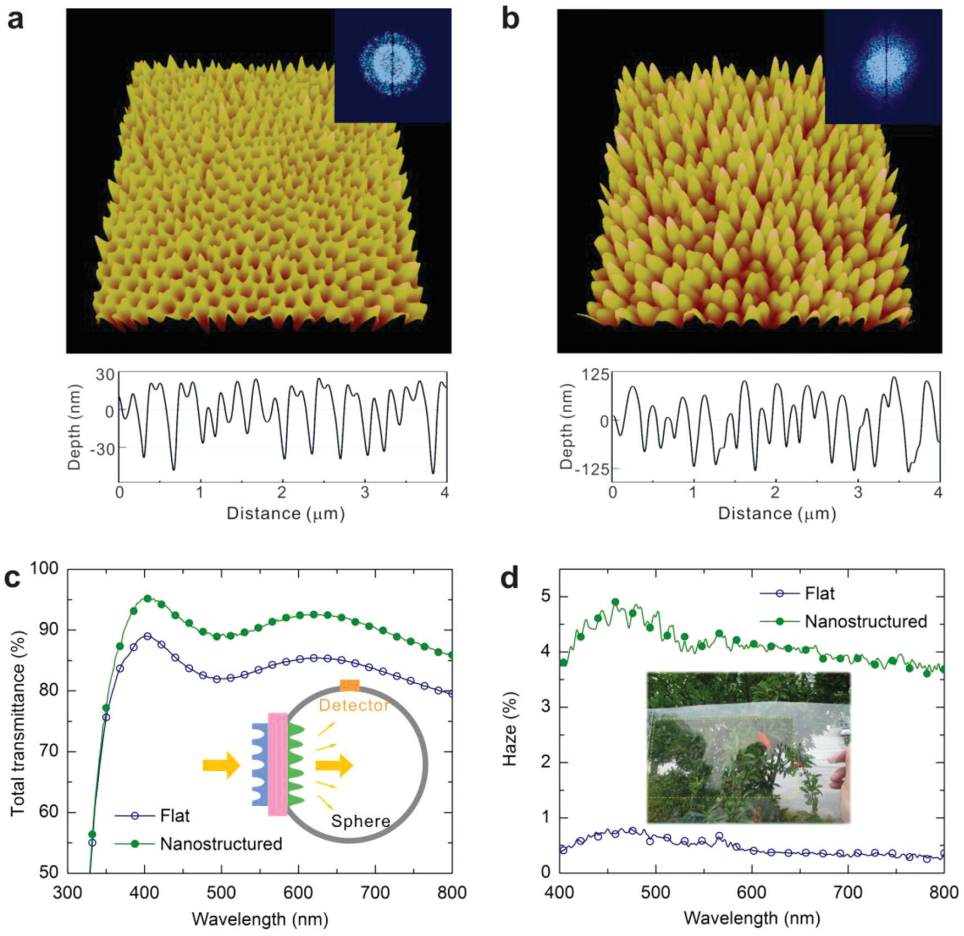

Figure 2. AFM images and optical properties of ITO glass substrates patterned with DANs. a,b) Perspective view of DAN transferred to PEDOT:PSS layer on ITO surface (a) and UV-curable resin on glass surface (b). Dimensions: 4 μm × 4 μm. The panels below indicate the depth profiles, showing the surface root-mean-square (RMS) roughness of about 6.5 nm. Insets show the fast Fourier transform (FFT) patterns of each image. c) Total transmittance of ITO glass substrate without and with DANs. Inset depicts the optical measurement configuration using an integrating sphere. d) Haze of ITO-glass substrate with DANs and an optical image of a plastic thin film coated with DANs (inset).

a continuously tapered morphology. Simultaneously, the fast Fourier transform (FFT) patterns (Figure 2a,b, inset) reveal an extended distribution of periodicity, which indicates that the DANs are suitable for broadband response and quasi-omnidirectional scattering.[33] The depth profiles show a pseudo sub-wavelength periodicity in the range from 150 to 350 nm with an average depth of 70 nm and 220 nm for iDAN and eDAN, respectively. Particularly, the characteristic depth of patterned PEDOT:PSS layer is much less than the layer thickness in OLEDs, and hence ensures the suppression of possible anomalies in the current flow. In addition, surface morphologies of the deposited organic layers confirm the conformal coating of the sequential deposition of organic layers and metal electrode on the patterned PEDOT:PSS layer (Supporting Information Figure S4), showing the extension of corrugated structures over all layers in OLEDs.

Figure 2c illustrates the optical transmittance of ITO glass substrates without and with DANs, which was measured by collecting both specular and diffuse lights using an integrating sphere for the propagation of incident light from the ITO side (Figure 2c, inset). Compared to the substrate only with a flat coating of PEDOT:PSS, the nanostructured ITO glass with DANs yields a higher value on transmittance with an enhancement of approximately 7% over the entire visible spectrum. The broadband optical nature on transmittance enhancement results from the broad distribution of periodicity and the gradient refractive index profiles of the sub-wavelength DAN pattern, which can fully interact with incident light and enable the reduced reflection loss.[35–37] Note that the increase in the transmittance spectra exhibits no apparent diversity over the visible wavelength range of 350–800 nm, suggesting the compatibility of DANs to extract the substrate-mode and waveguided light in white OLEDs without spectral distortion.

In addition to the total transmittance properties, the amount of light scattering present in DANs is determined by measuring the specular and diffuse transmission. The transmittance haze shows the percentage of light diffusely scattered compared to the total light transmitted, which is one of the pivotal features in the display applications.[35] Traditionally, the light scattering media incorporated into OLEDs always cause an additional haze (e.g., a haze value of about 80% for the microlens arrays), which conflicts with the requisites for high resolution

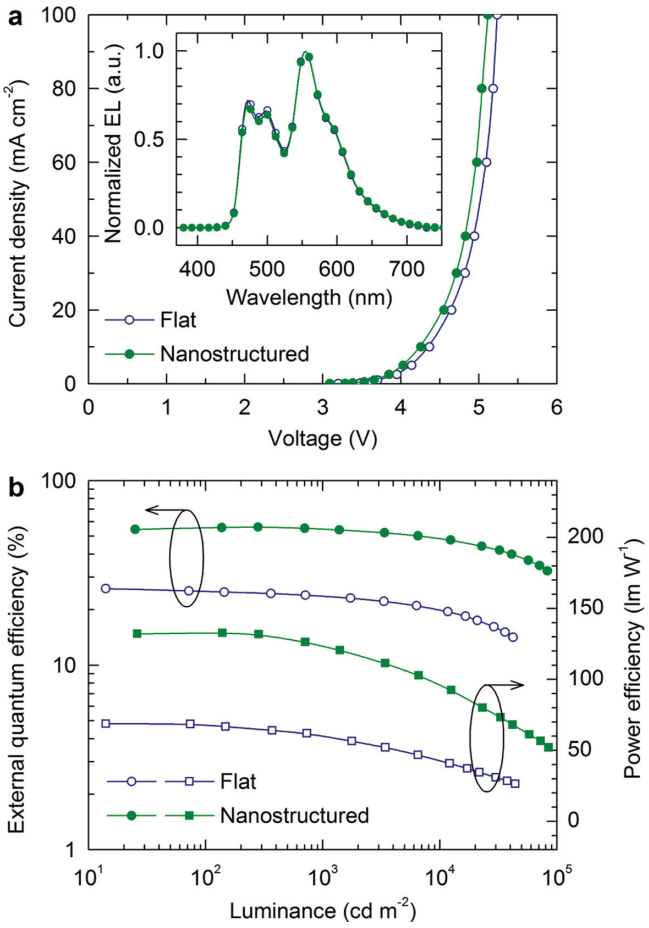

Figure 3. Device performance of white OLEDs. a) Current density–voltage (*J*–*V*) characteristics for devices with (filled circle) and without (open circle) DANs. Inset displays the normalized electroluminescence (EL) spectra obtained at 1000 cd m^{-2} in the direction normal to the glass substrate. b) External quantum efficiency and power efficiency as a function of luminance for the corresponding devices.

displays.[38] As depicted in Figure 2d, the average haze value of the ITO glass substrate with DANs is 4.15% over the visible spectrum as a comparison to 0.45% of the flat substrate. This result indicates that the DANs sustain not only the antireflective character for enhancing transmittance but also a low haze feature for keeping the transparency (e.g., an optical image of a plastic film coated with DANs in the inset of Figure 2d).

2.3. Device Performance

To examine the capability of DANs for light extraction, white OLEDs were constructed with a structure illustrated in Figure 1. Prior to the incorporation of DANs, we first focused on reducing the energetic and Ohmic losses that occur during the electron-photon conversion. A close-up view of the organic emitter in Figure 1b reveals a multilayer energy cascade structure with the insertion of an ultrathin TCTA interlayer and an n-doped electron injection layer of LiF:TmPyPB. The multilayer emitter is nearly barrier-free with the reduction of Ohmic losses on a negligible level, which can energetically facilitate hole transport from TAPC to FIrpic:mCP and electron transport through TmPyPB to PO-01:mCP, respectively. The performances of white OLEDs with a flat structure confirm a drastic decrease in operating voltage and thereby an improvement in efficiency, in which the η_{EQE} and η_{PE} at a luminance of 1000 cd m^{-2} are optimized to 23.6% and 60.0 lm W^{-1} with an operating voltage below 4 V (Supporting Information Figure S5).

Upon optimization of the emitter for energy-efficient exciton generation, white OLEDs with and without DANs were fabricated (see Experimental Section for details), and their performance characteristics are compared in **Figure 3**. Current density is plotted versus operating voltage in Figure 3a, showing a slightly reduced operating voltage for the device with DANs. The improved electrical property is mainly due to a stronger electric field distribution in the corrugated structure,[7] and also implies an excellent contact between nanostructured PEDOT:PSS layer and the subsequently deposited organic emitter. In addition, it was verified that the use of DANs has no influence on the device stability (Supporting Information Figure S6). The electroluminescence (EL) spectra of devices with and without DANs (Figure 3a, inset) display a negligible change in the spectral shape, and the corresponding Commission Internationale d'Eclairage (CIE) coordinates (*x*, *y*) are slightly shifted from (0.347, 0.461) to (0.343, 0.460) with the use of DANs, indicating no grating effects and a wavelength-independent response.

The η_{EQE} and η_{PE} of devices without and with DANs are plotted as functions of luminance in Figure 3b. The η_{EQE} and η_{PE} values, as well as the enhancement ratios relative to that of the flat device are summarized in **Table 1**. It is obvious that the use of DANs can drastically increase the light extraction and thus the device efficiency because the difference in operating voltages at 1000 cd m^{-2} for devices with and without DANs is less than 0.2 V. Note that the enhanced light extraction caused by DANs is the combined effect of iDAN and eDAN, both of which can effectively contribute to the increase in light extraction efficiency without spectral distortion (Supporting Information Figure S7). The use of iDAN promotes the out-coupling of the waveguide-mode light from the organic layers and ITO electrode into the glass substrate,[5] while the eDAN can enable the extraction of light trapped in glass due to total internal reflection.[4] The peak η_{EQE} and η_{PE} values of the white OLED with DANs are recorded as 56.1% and 132.8 lm W^{-1}, respectively, which are over two times those of the device constructed on a

Table 1. Efficiency comparison for white OLEDs without and with DANs.

Device structure	η_{PE} (maximum) [lm W^{-1}]	η_{EQE} (maximum) [%]	η_P (at 1000 cd m^{-2}) [lm W^{-1}]	η_{EQE} (at 1000 cd m^{-2}) [%]	η_{EQE} enhancement
Flat	68.8	26.0	60.0	23.6	1
Nanostructured	132.8	56.1	123.4	54.6	2.31

flat substrate. Moreover, the nanostructured device still maintains η_{EQE} = 54.6% and η_{PE} = 123.4 lm W^{-1} at a luminance of 1000 cd m^{-2}, which are among the highest reported efficiencies for white OLEDs in the scientific literature (Supporting Information Table S1). The efficiency of white OLEDs can be increased further by replacing the commonly used glass (ni = 1.5) with a high-refractive-index substrate to extract more light trapped in the waveguide mode.[2,3]

Furthermore, it is noteworthy that the nanostructured device structure designed here is featured by an extremely small roll-off in efficiency as well as excellent color stability at high luminance. The device with DANs yielded striking η_{PE} values of 106.5 lm W^{-1} and 96.1 lm W^{-1} at 5000 cd m^{-2} and 10 000 cd m^{-2}, respectively (Figure 3b), which iares accompanied with a luminance-independent EL spectrum over a broad range from 1000 to 30 000 cd m^{-2} (Supporting Information Figure S8). These features are a great improvement towards the current applications of flat panel displays and general lighting at high luminance (3000–5000 cd m^{-2}), which is usually challenging for phosphorescent OLEDs due to the pronounced efficiency roll-off and luminance-dependent color shift.

2.4. Angular Dependency

For high-quality white lighting applications, the color stability with increasing viewing angle is indispensable. **Figure 4** shows the angular dependence of emission characteristics of the devices with and without DANs. It is apparent that the emission for the device with DANs (Figure 4a) keeps a nearly identical spectral shape with increasing the viewing angle, resulting in a consistent white color. On the contrary, diverse EL spectra are observed in the counterpart with a flat device architecture (Figure 4b). The use of DANs causes a stronger side emission than that of the flat device, where the latter yields a Lambertian intensity distribution (Figure 4c). Correspondingly, the CIE color coordinates (Figure 4d) are far more stable with viewing angle for the device with DANs than for the flat structure. The changes of CIE coordinates (Δx, Δy) from 0° to 80° are (0.005, 0.004) and (0.007, 0.021) for the devices with and without DANs, respectively. The improved angular dependence of color stability can be attributed to the redirected emission over all azimuthal directions due to the excellent capability of quasi-omnidirectional light extraction of DANs for use in full-color OLEDs.[38–40] Additionally, the color stability can be estimated by the color shift (CS), which is defined as the Euclidean distance between two color points under certain angle and under surface normal (0°) in the CIE 1976 (u', v') color space.[41] Accordingly, the CS can be expressed as

$$CS(\theta) = \sqrt{(u'(\theta) - u'(0^\circ))^2 + (v'(\theta) - v'(0^\circ))^2} \quad (1)$$

where θ denotes the angle at which the chromaticity is measured with $0° < \theta \leq 90°$. Given that a lighting source shows omnidirectional color uniformity, no color variation is expected, showing a dot in the origin of the polar coordinate system. The farther the distance away from the origin, the more serious color shift. The device with DANs yields a maximum CS value

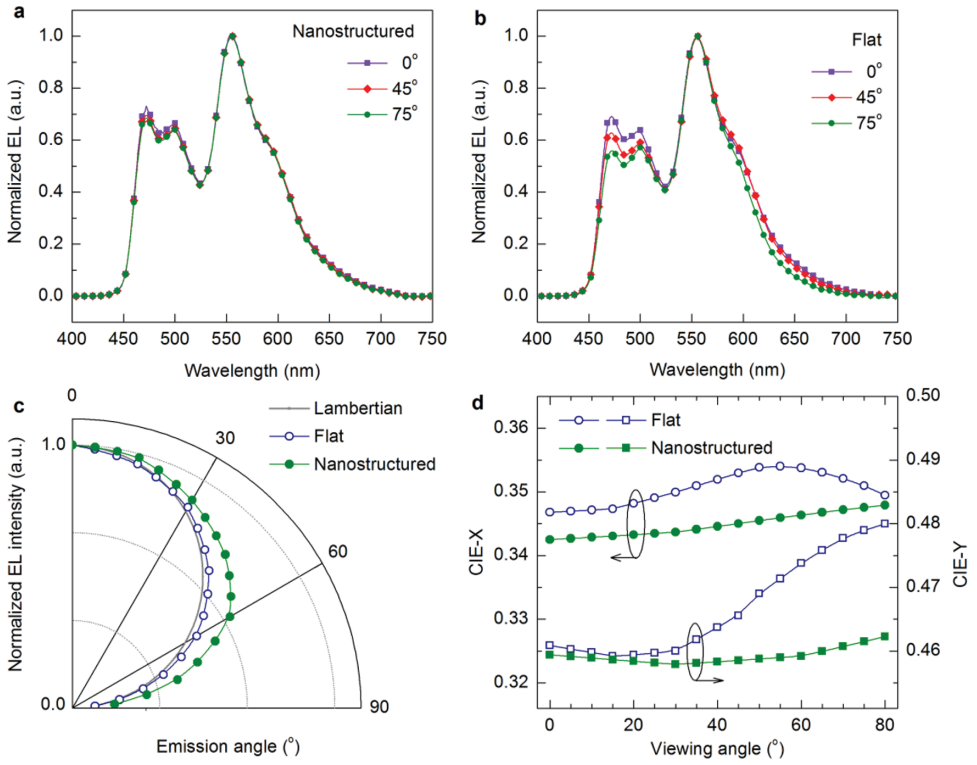

Figure 4. Angular dependence of EL performance for white OLEDs. a,b) Normalized EL spectra of white OLEDs with (a) and without (b) nanostructures for various viewing angles. c) Normalized angle-dependent emission intensities from devices with and without DANs. The ideal Lambertian emission pattern is shown as a guide to the eye. d) CIE color coordinates as a function of viewing angles.

of about 0.0028 at a viewing angle of 80° (Supporting Information Figure S9), revealing a better angular dependence of the color stability compared to a corresponding device with a flat structure (with a value of 0.0075). According to the definition of color spatial uniformity for typical white emission, the deviation on CIE 1976 (u', v') diagram should be within 0.004 from the weighted average point.[42] The resulting white OLEDs with DANs therefore fully satisfy the criteria of white emissions, which ameliorate the undesirable angle-dependent issues.

2.5. Theoretical Modeling

To elucidate the light extraction nature of DANs in OLEDs, we perform the optical modeling calculations using finite difference time domain (FDTD) and rigorous coupled wave analysis (RCWA) methods (see Experimental Section for the detailed description of the optical modeling). **Figure 5**a displays the waveguide modes in the device with a flat structure using the FDTD methods, including two transverse electric modes (TE_0 and TE_1) and three transverse magnetic modes (TM_0, TM_1 and TM_2). For the TE modes, the maximum field intensity of the TE_0 mode is mainly located on the ITO layer, while the TE_1 mode shows the highest field distribution near PEDOT:PSS/organic interface. For the TM modes, the TM_0 and TM_2 modes have maximum field intensities at organic/Al and glass/air interfaces, respectively, with a wide distribution of the TM_1 mode across all the layers. Since the light extraction efficiency of the waveguide modes is mostly dependent on the distribution of the optical field intensity along the corrugated region,[7,43] each TE or TM mode is expected to be out-coupled by the continuously tapered morphology profile of PEDOT:PSS/organic, glass/air, as well as organic/Al interfaces due to the widespread periodicities in DANs. Figure 5b presents the simulated dispersion diagram of optical intensity for TM polarization in the device with DANs using RCWA method. Extraordinary optical absorption spectra as a function of the fill factor and wavelength were also calculated (Supporting Information Figure S10), in which large-scale absorption occurs with the dispersed fill factors. A wide distribution of optical intensity is observed when ranging the wavelengths from 400 to 800 nm along with the broad periodicities of about 100 to 400 nm.

To further understand the extraction of optical modes, we proceeded to analyze cross-coupling mechanism with a hybrid plasmon-waveguide model.[44,45] Figure 5c,d show the calculated absorption spectra as the function of the frequency and wave vector k_x in the first Brillouin zone for TE and TM polarized lights, respectively. The phenomenon of light coupling by waveguide modes is present under TE polarization (Figure 5c), whereas more comprehensive optical response occurs for TM polarization.[46] First, strongly damped localized surface plasmon (LSP) modes could be excited in consequence of nanostructured metal electrode in the device with DANs. The dispersed directions of the LSP mode gradually split into two branches, which originates from Rayleigh-Wood anomalies.[47] Second, strong interactions between LSP and

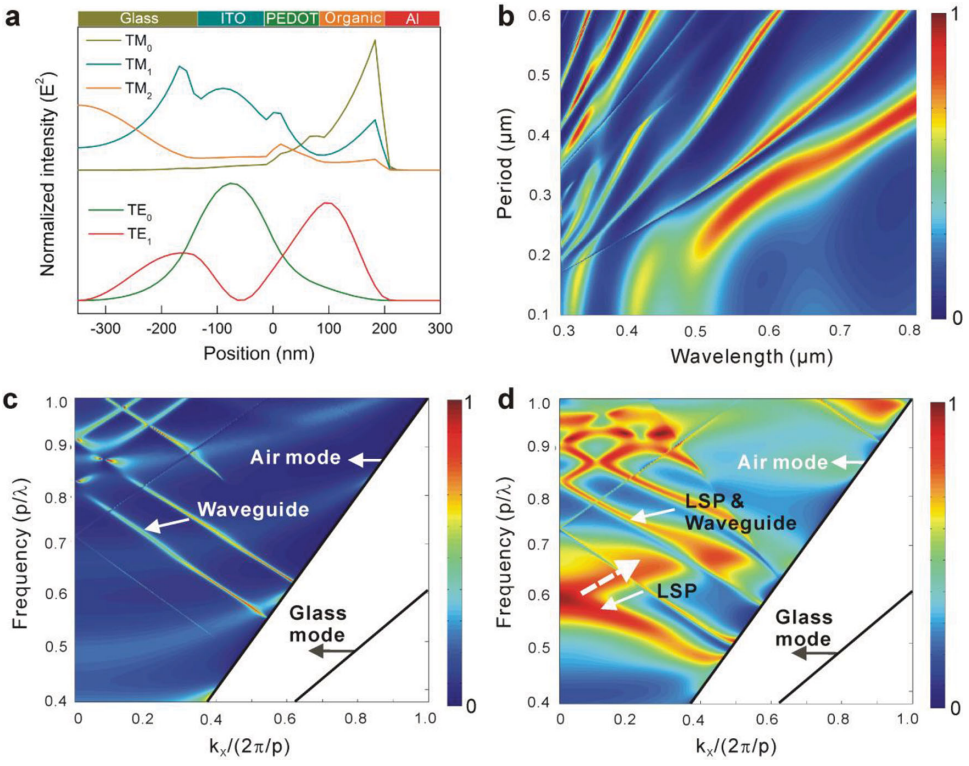

Figure 5. Optical simulations of white OLEDs. a) Normalized electric field intensity ($|E|^2$) for TE_0, TE_1 and TM_0, TM_1, TM_2 modes across the entire layers at a wavelength of 560 nm. b) Simulated dispersion relations of intensity field distributions as functions of structural periodicity and incident light wavelength. c,d) Calculated dispersions as a function of frequency and in-plane wave vector k_x in the first Brillouin zone for TE (c) and TM (d) polarized light in the device with DANs. White dashed arrow in (d) corresponds to the cross-coupling direction between plasmonic and waveguide modes.

photonic waveguide modes turn up, leading to a broadband and quasi-omnidirectional absorption enhancement. According to the previous reports,[48] enhanced light extraction could be attributed to the extraordinary absorption by the same optical resonant mode in the structure. As a consequence, the simulation results provide theoretical support that the enhanced light extraction over a wide range of angles and wavelengths is attributed to the excitation of hybrid plasmonic and waveguide modes in the device with DANs.

3. Conclusions

In summary, high-performance white OLEDs are demonstrated by implementing DANs for broadband quasi-omnidirectional light extraction and allowing energy-efficient photon generation in a multilayer energy cascade structure. The DANs are advantageous to manufacturing compatibility for large-area, flexible and low-cost electronic devices and are capable of light extraction with broad spectral response and directional randomness. The external quantum efficiency and power efficiency are increased to 54.6% and 123.4 lm W^{-1} at a luminance of 1000 cd m^{-2}. An extremely small roll-off in efficiency at high luminance is also obtained, yielding a striking value of 106.5 lm W^{-1} at 5000 cd m^{-2}. In addition to a substantial increase in efficiency, the DANs simultaneously offer the fantastic characteristics of angular color stability over the visible wavelength range with wide viewing angle. Note that the obstacles in color rendering index and lifetime issue related to the use of sky-blue phosphor FIrpic have to be solved for broad application of white OLEDs. We anticipate that the approach developed here is promising for accelerating the commercialization of large-scale and low-cost white OLED panels.

4. Experimental Section

Design and Characterization of DANs: The DANs used here were a combination of nano-honeycomb-style array patterned on PEDOT:PSS layer on an ITO surface and nanocone-style array on UV-curable resin film on the glass surface. The negative and positive DAN molds were prepared with an elastomeric perfluoropolyether (PFPE) material by a series of chemical etching and multitransfer process according to a previous report.[4] To prepare the iDAN on the ITO surface, a vacuum-assisted thermal PFPE nanoimprinting method was introduced on the basis of conventional SNILs (Supporting Information Figure S1). ITO-patterned glass substrates with a sheet resistance of 20 Ω per square were firstly cleaned using a routine process. The 100 nm-thick PEDOT:PSS film that was spin-coated from the aqueous solution (CLEVIOS P VP AI4083) onto the ITO glass substrate was covered in conformal contact with a flexible positive PFPE mold, and then transferred into a vacuum oven of ≈10^{-2} Torr with the controllable temperature at 80 °C. During the degassing process for 30 min, a uniform nanohoneycomb morphology was formed due to the synergistic powers of capillary force, vacuum pressure and thermal annealing. Finally, the preliminary nanopatterned PEDOT:PSS sample was annealed at 140 °C under atmospheric conditions for further 10 min to consummate the high-profile 3D sub-wavelength patterns and maintain the highly efficient electrical properties. To prepare the eDAN on the glass surface (Supporting Information Figure S1), the negative PFPE mold was applied to make conformal coating of positive cone-shaped topology after drop-casting the UV-curable resin (D10, PhiChem) on the glass surface. The UV-curable resin film was embossed under a constant pressure of 1.5 bar for 10 s with a UV illumination at light power intensity of 500 mJ cm^{-2} at a wavelength of 395 nm. The imprinting recipe was optimized by a systematic study of the imprinting time and pressure. Surface topology of DANs was characterized by AFM (Veeco Multimode V) in tapping mode. Optical transmittance measurements were carried out using an UV/vis/near-IR spectrometer (Perkin Elmer Lambda 750). For obtaining haze values, total transmittance and specular transmittance were collected with and without integrating sphere, respectively. The transmittance of air was taken and used as a baseline measurement. The haze of ITO/glass substrate with DANs was calculated by generating the transmittance values into the formula, haze = (total transmittance – specular transmittance)/total transmittance.

Device Fabrication and Measurement: The white OLEDs were fabricated by subsequently depositing the organic layers and a LiF (0.7 nm)/Al (100 nm) bilayer cathode onto the substrates by thermal evaporation with shadow mask in high vacuum chamber (base pressure ≈2×10^{-6} Torr), in which the deposition rate and film thickness were monitored by a quartz crystal oscillator. The device area is 10 mm^2. White OLEDs with and without DANs were fabricated at the same time to ensure consistent results (see Supporting Information Figure S2 for chemical structures used for OLEDs). The current density–voltage–luminance (*J–V–L*) characteristics and EL spectra of white OLED devices were measured simultaneously in air ambience using a programmable source meter (Keithley 2400) and a luminance meter/spectrometer (PhotoResearch PR655). The angular emission patterns were measured according to emission angles.

Theoretical Modeling and Simulation: The in-plane waveguide modes including TE and TM in OLEDs with DANs were simulated based on the rigorous electromagnetic theory through finite difference time domain (FDTD) approach by Lumerical FDTD Solutions 8.7.3. To find a rigorous solution to Maxwell's equations, the rigorous coupled wave analysis (RCWA) method was adopted to model the dispersion diagram as well as the near-field distribution of white OLEDs with DANs based on the optical calculation module (Rsoft DiffractMOD) from commercial software RSoft 8.1 (RSoft Design Group, Inc). For simplicity, hexagonal closely packed nanostructures with linearly tapered profile were representatively constructed instead of randomly distributed geometry, along with a simplified periodicity of 250 nm replacing the broad distributed periodicities. In the device modeling, the complex optical dielectric function of nanostructured Al were fitted using Drude-Lorentz model, and the frequency-dependent refractive index (*n*) and extinction cofficient (*k*) of the materials were measured experimentally using an alpha-SE Spectroscopic Ellipsometer.

Supporting Information

Supporting Information is available from the Wiley Online Library or from the author.

Acknowledgements

Q.-D.O. and L.Y. contributed equally to this work. The authors acknowledge financial support from the National Basic Research Program of China (Grant No. 2014CB932600, 2011CB808404), the National Natural Science Foundation of China (Nos 11474214, 91027041, 61107022), Jiangsu Science and Technology Department (No. BK20140053), Key Natural Science Foundation of the Higher Education Institutions of Jiangsu Province (No. 10KJA140048), and the project of the Priority Academic Program Development (PAPD) of Jiangsu Higher Education Institutions.

Received: June 19, 2014
Revised: July 31, 2014
Published online: September 8, 2014

[1] J. Kido, M. Kimura, K. Nagai, *Science* **1995**, *267*, 1332.
[2] S. Reineke, F. Lindner, G. Schwartz, N. Seidler, K. Walzer, B. Lussem, K. Leo, *Nature* **2009**, *459*, 234.
[3] N. Li, S. Oida, G. S. Tulevski, S. J. Han, J. B. Hannon, D. K. Sadana, T. C. Chen, *Nat. Commun.* **2013**, *4*, 2294.
[4] L. Zhou, Q.-D. Ou, J.-D. Chen, S. Shen, J.-X. Tang, Y.-Q. Li, S.-T. Lee, *Sci. Rep.* **2014**, *4*, 4040.
[5] Y. Sun, S. R. Forrest, *Nat. Photonics* **2008**, *2*, 483.
[6] T.-H. Han, Y. Lee, M.-R. Choi, S.-H. Woo, S.-H. Bae, B. H. Hong, J.-H. Ahn, T.-W. Lee, *Nat. Photonics* **2012**, *6*, 105.
[7] W. H. Koo, S. M. Jeong, F. Araoka, K. Ishikawa, S. Nishimura, T. Toyooka, H. Takezoe, *Nat. Photonics* **2010**, *4*, 222.
[8] M. G. Helander, Z. B. Wang, J. Qiu, M. T. Greiner, D. P. Puzzo, Z. W. Liu, Z. H. Lu, *Science* **2011**, *332*, 944.
[9] Y. Zhou, C. Fuentes-Hernandez, J. Shim, J. Meyer, A. J. Giordano, H. Li, P. Winget, T. Papadopoulos, H. Cheun, J. Kim, M. Fenoll, A. Dindar, W. Haske, E. Najafabadi, T. M. Khan, H. Sojoudi, S. Barlow, S. Graham, J. L. Bredas, S. R. Marder, A. Kahn, B. Kippelen, *Science* **2012**, *336*, 327.
[10] H. Uoyama, K. Goushi, K. Shizu, H. Nomura, C. Adachi, *Nature* **2012**, *492*, 234.
[11] Q. Wang, D. Ma, *Chem. Soc. Rev.* **2010**, *39*, 2387.
[12] M. A. Baldo, D. F. O'Brien, Y. You, A. Shoustikov, S. Sibley, M. E. Thompson, S. R. Forrest, *Nature* **1998**, *395*, 151.
[13] Y. Sun, N. C. Giebink, H. Kanno, B. Ma, M. E. Thompson, S. R. Forrest, *Nature* **2006**, *440*, 908.
[14] Y.-S. Tyan, *J. Photonics Energy* **2011**, *1*, 011009.
[15] H. Sasabe, J. i. Takamatsu, T. Motoyama, S. Watanabe, G. Wagenblast, N. Langer, O. Molt, E. Fuchs, C. Lennartz, J. Kido, *Adv. Mater.* **2010**, *22*, 5003.
[16] J. P. Yang, Y. Xiao, Y. H. Deng, S. Duhm, N. Ueno, S. T. Lee, Y. Q. Li, J. X. Tang, *Adv. Funct. Mater.* **2012**, *22*, 600.
[17] a) B. Z. Tang, X. Zhan, G. Yu, P. P. S. Lee, Y. Liu, D. Zhu, *J. Mater. Chem.* **2001**, *11*, 2974; b) M. F. Lo, T. W. Ng, H. W. Mo, C. S. Lee, *Adv. Funct. Mater.* **2013**, *23*, 1718.
[18] a) J. Y. Kim, T. Yasuda, Y. S. Yang, C. Adachi, *Adv. Mater.* **2013**, *25*, 2666; b) K.-H. Kim, C.-K. Moon, J.-H. Lee, S.-Y. Kim, J.-J. Kim, *Adv. Mater.* **2014**, *26*, 3844.
[19] V. Bulović, V. B. Khalfin, G. Gu, P. E. Burrows, D. Z. Garbuzov, S. R. Forrest, *Phys. Rev. B* **1998**, *58*, 3730.
[20] A. Chutinan, K. Ishihara, T. Asano, M. Fujita, S. Noda, *Org. Electron.* **2005**, *6*, 3.
[21] S. Y. Kim, W. I. Jeong, C. Mayr, Y. S. Park, K. H. Kim, J. H. Lee, C. K. Moon, W. Brütting, J. J. Kim, *Adv. Funct. Mater.* **2013**, *23*, 3896.
[22] S. Möller, S. Forrest, *J. Appl. Phys.* **2002**, *91*, 3324.
[23] G. Schwartz, M. Pfeiffer, S. Reineke, K. Walzer, K. Leo, *Adv. Mater.* **2007**, *19*, 3672.
[24] J. P. Yang, Q. Y. Bao, Z. Q. Xu, Y. Q. Li, J. X. Tang, S. Shen, *Appl. Phys. Lett.* **2010**, *97*, 223303.
[25] J. Lim, S. S. Oh, D. Y. Kim, S. H. Cho, I. T. Kim, S. H. Han, H. Takezoe, E. H. Choi, G. S. Cho, Y. H. Seo, S. O. Kang, B. Park, *Opt. Express* **2006**, *14*, 6564.
[26] Y. Do, Y. C. Kim, Y. W. Song, C. O. Cho, H. Jeon, Y. J. Lee, S. H. Kim, Y. H. Lee, *Adv. Mater.* **2003**, *15*, 1214.
[27] E. Matioli, S. Brinkley, K. M. Kelchner, Y.-L. Hu, S. Nakamura, S. DenBaars, J. Speck, C. Weisbuch, *Light: Sci. Appl.* **2012**, *1*, e22.
[28] J. M. Ziebarth, A. K. Saafir, S. Fan, M. D. McGehee, *Adv. Funct. Mater.* **2004**, *14*, 451.
[29] C. Xiang, W. Koo, F. So, H. Sasabe, J. Kido, *Light: Sci. Appl.* **2013**, *2*, e74.
[30] Y. G. Bi, J. Feng, Y. F. Li, X. L. Zhang, Y. F. Liu, Y. Jin, H. B. Sun, *Adv. Mater.* **2013**, *25*, 6969.
[31] J. A. Schuller, E. S. Barnard, W. Cai, Y. C. Jun, J. S. White, M. L. Brongersma, *Nat. Mater.* **2010**, *9*, 193.
[32] P. A. Hobson, S. Wedge, J. A. E. Wasey, I. Sage, W. L. Barnes, *Adv. Mater.* **2002**, *14*, 1393.
[33] E. R. Martins, J. Li, Y. Liu, V. Depauw, Z. Chen, J. Zhou, T. F. Krauss, *Nat. Commun.* **2013**, *4*, 2665.
[34] a) S. Braun, W. R. Salaneck, M. Fahlman, *Adv. Mater.* **2009**, *21*, 1450; b) J. X. Tang, C. S. Lee, S. T. Lee, *J. Appl. Phys.* **2007**, *101*, 064504; c) M. Oehzelt, N. Koch, G. Heimel, *Nat. Commun.* **2014**, *5*, 4174.
[35] H. K. Raut, V. A. Ganesh, A. S. Nair, S. Ramakrishna, *Energy Environ. Sci.* **2011**, *4*, 3779.
[36] J. A. Hiller, J. D. Mendelsohn, M. F. Rubner, *Nat. Mater.* **2002**, *1*, 59.
[37] Y. F. Huang, S. Chattopadhyay, Y. J. Jen, C. Y. Peng, T. A. Liu, Y. K. Hsu, C. L. Pan, H. C. Lo, C. H. Hsu, Y. H. Chang, C. S. Lee, K. H. Chen, L. C. Chen, *Nat. Nanotechnol.* **2007**, *2*, 770.
[38] C. Lee, J. J. Kim, *Small* **2013**, *9*, 3858.
[39] W. Gaynor, S. Hofmann, M. G. Christoforo, C. Sachse, S. Mehra, A. Salleo, M. D. McGehee, M. C. Gather, B. Lüssem, L. Müller-Meskamp, P. Peumans, K. Leo, *Adv. Mater.* **2013**, *25*, 4006.
[40] J.-W. Shin, D.-H. Cho, J. Moon, C. W. Joo, S. K. Park, J. Lee, J.-H. Han, N. S. Cho, J. Hwang, J. W. Huh, H. Y. Chu, J.-I. Lee, *Org. Electron.* **2014**, *15*, 196.
[41] A. Isphording, M. Pralle, *Org. Electron.* **2010**, *11*, 1916.
[42] T. Komoda, H. Tsuji, K. Yamae, K. Varutt, Y. Matsuhisa, N. Ide, *SID11 Dig.* **2011**, 1056.
[43] J. M. Ziebarth, M. D. McGehee, *J. Appl. Phys.* **2005**, *97*, 064502.
[44] A. Christ, S. Tikhodeev, N. Gippius, J. Kuhl, H. Giessen, *Phys. Rev. Lett.* **2003**, *91*, 183901.
[45] J. Zhang, W. Bai, L. Cai, X. Chen, G. Song, Q. Gan, *Appl. Phys. Lett.* **2011**, *98*, 261101.
[46] Y. Bai, J. Feng, Y.-F. Liu, J.-F. Song, J. Simonen, Y. Jin, Q.-D. Chen, J. Zi, H.-B. Sun, *Org. Electron.* **2011**, *12*, 1927.
[47] A. Christ, T. Zentgraf, J. Kuhl, S. Tikhodeev, N. Gippius, H. Giessen, *Phys. Rev. B* **2004**, *70*, 125113.
[48] H. Liu, P. Lalanne, *Nature* **2008**, *452*, 728.